ResearchGate

See discussions, stats, and author profiles for this publication at: https://www.researchgate.net/publication/49825134

Synthesis and Growth Mechanism of Iron Oxide Nanowhiskers

ARTICLE *in* NANO LETTERS · FEBRUARY 2011

Impact Factor: 13.59 · DOI: 10.1021/nl200136j · Source: PubMed

CITATIONS
45

READS
102

9 AUTHORS, INCLUDING:

Soubantika Palchoudhury
University of Tennessee at Chattanooga
21 PUBLICATIONS **231** CITATIONS
SEE PROFILE

Wei An
Shanghai University of Engineering Science
47 PUBLICATIONS **1,064** CITATIONS
SEE PROFILE

Nitin Chopra
University of Alabama
22 PUBLICATIONS **2,194** CITATIONS
SEE PROFILE

Available from: Wei An
Retrieved on: 17 January 2016

NANO LETTERS

LETTER

pubs.acs.org/NanoLett

Synthesis and Growth Mechanism of Iron Oxide Nanowhiskers

Soubantika Palchoudhury,[†] Wei An,[†] Yaolin Xu,[†] Ying Qin,[‡] Zhongtao Zhang,[†] Nitin Chopra,[§] Robert A. Holler,[∥] C. Heath Turner,[*,†] and Yuping Bao[*,†]

[†]Chemical and Biological Engineering, [‡]Alabama Institute for Manufacturing Excellence, [§]Metallurgical and Materials Engineering and Center for Materials for Information Technology, and [∥]Central Analytical Facility, The University of Alabama, Tuscaloosa, Alabama, 35487 United States

Supporting Information

ABSTRACT: Iron oxide nanowhiskers with dimensions of approximately 2 × 20 nm were successfully synthesized by selectively heating an iron oleate complex. Such nanostructures resulted from the difference in the ligand coordination microenvironments of the Fe(III) oleate complex, according to our electronic structure calculations and thermogravimetric analysis. A ligand-directed growth mechanism was subsequently proposed to rationalize the growth process. The formation of the nanowhiskers provides a unique example of shape-controlled nanostructures, offering additional insights into nanoparticle synthesis.

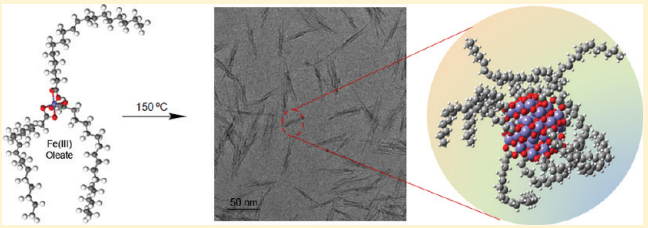

KEYWORDS: Iron oxide nanowhiskers, ligand-directed growth, electronic structure calculation of complexes, iron oxide nanoclusters

Anisotropic nanostructures have attracted much attention in various applications because of their unique electronic, magnetic, and optical properties.[1−3] In particular, the synthesis of one-dimensional (1D) metallic and semiconductor nanostructures has been well documented.[3−5] Most recently, ultrathin (∼2 nm) nanowires,[6] such as Au,[7−10] FePt,[11] and oxides,[12,13] have attracted much interest. In contrast, only few studies of 1D iron oxide magnetic nanoparticles have been reported (e.g., iron oxide nanobars[14] and nanowires[15]). Spherical iron oxide nanoparticles have been primarily explored in targeted drug delivery, localized therapy, or as contrast agents for magnetic resonance imaging (MRI).[16,17] A recent study of 1D iron oxide nanoworms showed long blood circulation time, enhanced retention at tumor sites, and improved targeting efficiency,[18] which suggests that anisotropic iron oxide nanoparticles could potentially lead to further advancement in biomedical applications.

The synthetic approach to iron oxide spheres has been intensively focused on the thermal decomposition of iron(III) oleate complexes due to its great reproducibility and control of the physical parameters.[19] In this method, the Fe(III) oleate precursor is typically heated up to over 300 °C, producing different-sized spherical nanoparticles with a narrow size distribution. Cubic and bipyramid-shaped particles were also reported using this method as a result of the selective absorption of impurity ions, such as Cl^-, Na^+, or oleate.[20−26] So far, the formation of ultrathin, 1D iron oxide nanoparticles has not been reported.

Even though the decomposition of the iron oleate complex is widely used for the synthesis of iron oxide nanoparticles, few mechanistic studies are available to understand the growth process. Hyeon[27] proposed that the dissociation of the first oleate ligand at around 200−240 °C triggered the nucleation event, followed by nanoparticle growth through the decomposition of the two remaining ligands above 300 °C. However, it has been rather difficult to conclusively confirm the dissociation process of the iron oleate complex. A recent density functional theory (DFT) electronic structure calculation of iron carboxylate complexes showed different dissociation temperatures of the three carboxylate ligands.[28] The first and the second ligands have similar dissociation temperatures, while the dissociation temperature of the third ligand was significantly higher.[28] The calculations further proposed the formation of an Fe−O bond between the third ligand and the iron center. Unfortunately, an understanding of the chemical microenvironments of these three ligands and their effects on the nanostructure formation is still lacking.

In this Letter, we report the synthesis of ultrathin iron oxide nanowhiskers, based on an understanding of the precursor chemistry. Our DFT calculations of the Fe(III) oleate complex predict a large difference among the binding energies of the three ligands. Experimentally, such a difference was reflected by the distinct weight losses of the thermogravimetric analysis (TGA) plot of the Fe(III) oleate complex. The different bindings allowed us to selectively decompose the more weakly bound ligands at 150 °C, forming iron oxide nanoclusters through ligand-directed growth. This study provides a unique example of shape-controlled iron oxide nanoparticles, which demonstrates the importance of the chemical microenvironments,

Received: November 19, 2010
Published: February 10, 2011

ACS Publications © 2011 American Chemical Society

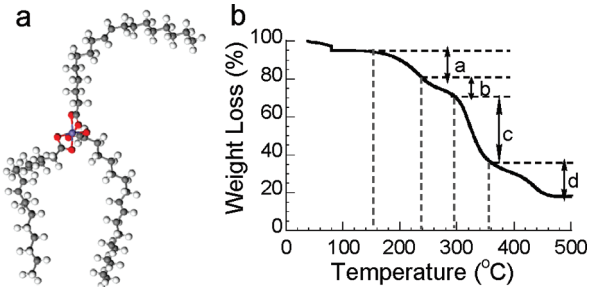

Figure 1. The iron oleate complex. (a) An optimized structure based on DFT calculations and (b) a TGA plot.

offering additional insight into nanoparticle synthesis mechanisms.

A typical synthesis of iron oxide nanowhiskers starts with the preparation of the iron oleate complex followed by selective decomposition at 150 °C. The ligand coordination environments of the Fe(III) oleate complex were first investigated using DFT electronic structure calculations and TGA measurements. Figure 1a shows the optimized geometric structure of the Fe(III) oleate complex obtained from our electronic structure calculations. This complex has a FeO_6 quasi-octahedral core structure with a nonequivalent arrangement of the three ligands: two symmetric bonds and one asymmetric bond. The calculated binding energies of two of those ligands are very similar (7.0 and 10.5 eV) but the binding energy of the third one is much higher (39.2 eV). The lower binding energies are likely associated with the two symmetric ligands with a weak binding to the Fe(III) center. These calculated binding energies agree well with previously reported simulations of Fe(III) carboxylate complexes, which showed two ligands with low-dissociation temperatures and one with a much higher dissociation temperature.[28]

The thermal decomposition behavior of the Fe(III) oleate complex was experimentally studied using TGA measurements, which provide an indirect prediction of the ligand binding strength of the complex. Figure 1b shows a TGA plot obtained at a constant heating rate of 5 °C/min. The initial weight loss before 100 °C was due to the evaporation of the adsorbed solvents from the synthesis of the iron oleate complex. The second distinct weight loss started at around 150 °C and continued until 230 °C (Figure 1b, region a), and this loss was attributed to the dissociation of the two symmetric ligands with lower binding energies. The small percentage weight loss in the range of 230−295 °C is from the decomposition of the third ligand (Figure 1b, region b). During these two steps of ligand decomposition, the weight losses are mainly from the release of CO_2 gas with a decomposition ratio close to 2:1. The decomposition ratio agrees very well with our DFT calculations that two ligands have lower binding energies. The chemical reaction associated with this process can be reasonably explained using the ketonic decarboxylation reaction (eq 1), as suggested in many other heating studies of iron carboxylate.[29−31] The detailed reaction process is believed to occur through the decomposition and recombination of several radical species (e.g., $RCOO^{\bullet}$ and $RC^{\bullet}O$). The continuous weight loss between 295 and 345 °C was attributed to desorption of the decomposed ligands (Figure 1b, region c). Finally, vaporization of all organic

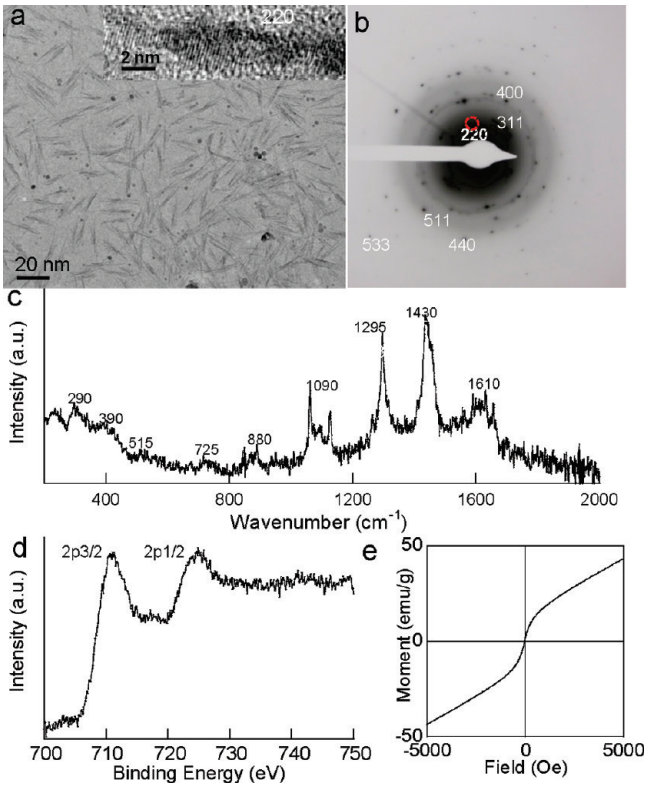

Figure 2. Iron oxide nanowhiskers. (a) Bright-field TEM image and HRTEM (inset), (b) electron diffraction pattern, (c) a Raman spectrum, (d) Fe 2p core-level spectrum, and (e) room-temperature M-H curve.

compounds resulted in further weight losses above 350 °C (Figure 1b, region d)

$$\mathrm{Fe(OOCR)_3} \xrightarrow{\Delta} \mathrm{RCOR + RCOOFe - O + CO_2} \quad (1)$$

To obtain further insight into the weight loss at 150 °C, TGA analysis at a slower heating rate (1 °C/min) and an isothermal analysis at 150 °C for 3.5 h were performed (Supporting Information Figure S1). The TGA plot at a slower heating rate demonstrated the same weight loss onset at around 150 °C, but it continued until 200 °C, suggesting a slow decomposition process of the two symmetric ligands. The isothermal analysis performed at 150 °C reached a weight loss of 9% after approximately 2.5 h also indicating a slow dissociation process of the two symmetric ligands while heating. The weight loss was primarily due to the release of CO_2 gas from the ketonic decarboxylation reaction. The isothermal TGA analysis also suggested the high stability of the third ligand at 150 °C, where continuous weight loss was not observed.

Our DFT calculations and TGA measurement suggest a difference in the ligand coordination environments within a Fe(III) oleate complex, which has not previously studied. Accordingly, a synthesis was performed to selectively decompose the more weakly bound ligands at 150 °C, a temperature that was previously believed not to facilitate nanoparticle formation.[19,25,32] Interestingly, iron oxide nanowhiskers with dimensions of approximately 2 × 20 nm were formed after 2.5 h of heating (Figure 2a). A high-resolution transmission electron microscopy (TEM) image of a single nanowhisker showed clear lattice fringes, indicating the crystallinity of these nanostructures

dx.doi.org/10.1021/nl200136j |*Nano Lett.* 2011, 11, 1141–1146

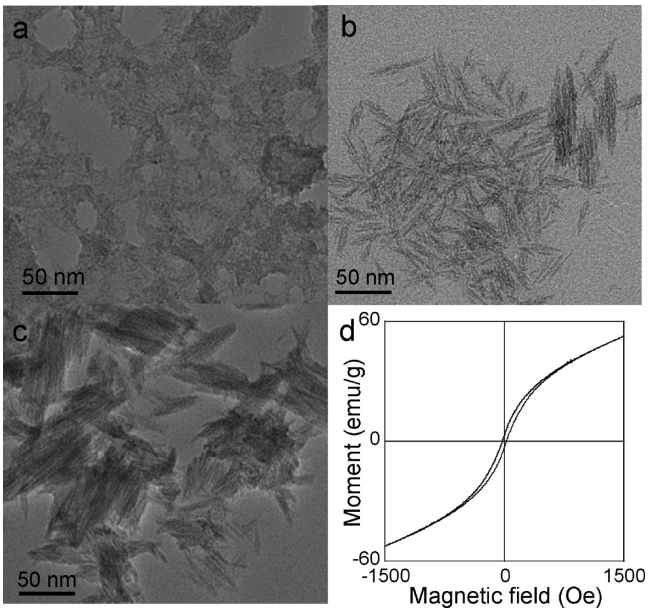

Figure 3. Time-dependent morphology evolution of nanowhiskers. (a) 0.5 h, (b) 6 h, (c) 22 h, and (d) the M-H curve of assembled nanowhisker bundles.

(Figure 2a, inset). The calculated interfringe distance of 0.298 nm was close to the interfringe distance of the {220} plane of the cubic iron oxide spinel structure. The electron diffraction pattern collected on several nanowhiskers agreed well with the Fe_2O_3 crystal phase (Figure 2b). The observed diffraction dots rather than rings also indicated the crystallinity of these nanowhiskers. Unfortunately, the X-ray diffraction scan did not allow us to confirm their crystal phases due to the significant size broadening (Supporting Information Figure S2).

To further confirm the crystal phase, a Raman spectrum of these nanowhiskers was collected using a Bruker Senterra system (Figure 2c). The absence of the major feature peak of Fe_3O_4 at around 670 cm^{-1} suggests that these nanowhiskers are not magnetite phase;[33] in contrast, the main peaks of 725, 1295, 1430 cm^{-1} can be readily assigned to the γ-Fe_2O_3 phase.[34] These iron oxide nanostructures are unlikely in the α-Fe_2O_3 phase, because the Raman peaks for α-Fe_2O_3 would be much sharper, especially in the region of 200−400 cm^{-1}.[33] The broad peak around 1610 cm^{-1} corresponds to adsorbed moisture or −OH groups.

Additionally, XPS analysis was performed to confirm the Fe valence states of the nanowhiskers. This technique has been utilized as an effective tool for differentiating magnetite (Fe_3O_4) from maghemite (γ-Fe_2O_3).[35] Figure 2d shows the core-level XPS pattern of the nanowhiskers in the Fe 2p region. The two major peaks at 710.7 and 725.0 eV correspond to the $2p_{3/2}$ and $2p_{1/2}$ core levels of iron oxide. Small satellite signals around 718.0, 730.0, and 745.0 eV were an indicator of γ-Fe_2O_3 rather than Fe_3O_4, as suggested in ref 35. Independently, another reported XPS study of iron oxide nanoparticles utilized the shoulder peak between Fe $2p_{3/2}$ and Fe $2p_{1/2}$ to confirm the phase of γ-Fe_2O_3.[36] This shoulder peak can be identified in our XPS pattern as well.

The magnetization versus applied field (M-H) curve of these nanowhiskers showed mixed superparamagnetic and paramagnetic signals without saturation (Figure 2e). The observed magnetic property is a result of the high surface-to-volume ratio

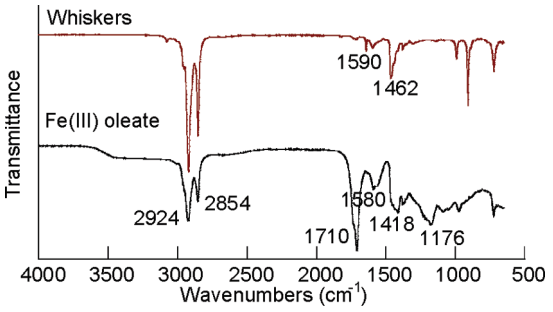

Figure 4. FTIR spectra of the iron oleate complex precursor (bottom) and iron oxide nanowhiskers synthesized with OA (top).

and surface iron-ligand complexation. Compared to spherical- or cubic-shaped nanoparticles, the thin nanowhiskers have much higher surface-to-volume ratios. Further, the high percentage of surface atoms was linked to oleate ligands through coordination bonds, behaving as iron complexes. The surface effects generate a magnetic "dead layer" on the nanoparticle surfaces, which is commonly observed in small magnetic nanoparticle systems.[37−41] Theoretical simulations also suggested that the dead layer is around 1 nm thick,[42] and this effect could be significant in high surface-to-volume ratio nanostructures, as observed in our nanowhisker system.

The growth process of the nanowhiskers was monitored by taking samples out of the reaction solution at different time intervals. These intermediate solutions were directly deposited on TEM grids without any wash or other treatments to capture the intermediate nanostructural morphologies (Figure 3). At 0.5 h, structures with no clear morphology on a dark background were observed (Figure 3a), and the nanowhiskers were not produced. As time goes by, the paste morphology starts breaking down, forming structures with 1D morphology at 1 h (Figure S3a, Supporting Information). At reaction time of 1.5 h, many nanowhiskers can be clearly observed (Figure S3b, Supporting Information). After 2.5 h (the normal reaction time), iron oxide nanowhiskers were the primary product, as seen in Figure 2a. The whisker morphology remained after 6 h of heating (Figure 3b). Unfortunately, continuous heating (22 h) led to the formation of assembled nanowhisker bundles or sheets (Figure 3c). Compared to the mixed paramagnetic and ferromagnetic signals of the isolated nanowhiskers, the nanowhisker bundles were ferromagnetic, as indicated by the open loop in the M-H curve (Figure 3d). But, the whisker morphology can still be clearly identified within the bundles, an indication of the nanowhisker stability at the reaction temperature.

The FTIR vibrational bands of carboxylic groups were utilized to study the surface coordination environments of the precursor complex and the nanowhiskers (Figure 4). The frequency difference, Δ, between the asymmetrical (ν_{as}) and symmetrical (ν_s) COO^- vibration for a metal carboxylate complex is an indicator of the nature of the coordination bonds, including monodentate (Δ = 200−300 cm^{-1}), bridging bidentate or ionic interactions (Δ = 110−200 cm^{-1}), and chelating bidentente (Δ <110 cm^{-1}).[43,44] The FTIR spectra of the iron oleate complex exhibited several characteristic IR bands of metal carboxylate, including 1710, 1580, 1418, and 1176 cm^{-1}. The band at 1710 cm^{-1} can be assigned to either free oleic acid[45] or the asymmetrical unidentate carboxylate.[47] The frequency difference of 162 cm^{-1} between the two characteristic bands of the iron oleate

dx.doi.org/10.1021/nl200136j |Nano Lett. 2011, 11, 1141–1146

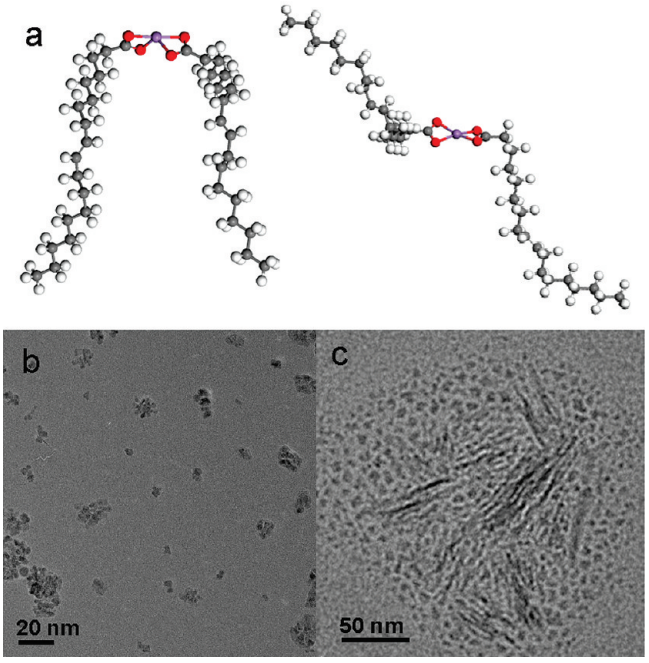

Figure 5. (a) Optimized structures of the Fe(II) oleate complex, (b) irregular particles from decomposition of Fe(II) oleate, and (c) a mixture of spherelike nanoparticles and nanowhiskers from the decomposition of the Fe(II) and Fe(III) oleate complex mixture.

complex (1580 and 1418 cm^{-1}) indicates the existence of a bridging coordination bond. The bridging coordination mode was also reported in other iron carboxylate compounds.[46] The experimentally estimated bridging bond mode can be understood by the binding energy differences of the bidentate bonds, according to the electronic structure calculations or the occurrence of multiple Fe nuclei species in the precursor.

In contrast, the band at 1710 cm^{-1} for iron oxide nanowhiskers disappeared, suggesting the remaining ligands were linked to the nanoparticle surfaces. The frequency difference of 128 cm^{-1} also falls within the range of a bridging coordination bond, indicating little change in the ligand coordination environments during the nanowhisker formation.

A temperature-dependent study was performed to further understand the formation process of these nanowhiskers, in particular the role of the third ligand with stronger binding. A reaction conducted at 100 °C did not produce whiskerlike morphology, forming dark pasty materials (Supporting Information Figure S4a); while nanowhiskers were observed at 180 °C (Supporting Information Figure S4b). Interestingly, the reaction at 230 °C produced a mixture of nanowhiskers and small irregular nanoparticles (Supporting Information Figure S4c). The formation of the small irregular nanoparticles is likely due to the further decomposition of the remaining ligand. Finally, spherical nanoparticles were observed for a reaction conducted above 300 °C (Supporting Information Figure S4d), as commonly reported in the literature. These observations suggest that the remaining third ligand is critical for the nanowhisker formation, because the third ligand could start decomposing above 200 °C according to the TGA plot (Supporting Information Figure S1a).

To further investigate the role of the third ligand, the Fe(II) oleate and Fe(II)/Fe(III) oleate mixture were prepared in a similar way but with inert gas protection. Subsequently, we performed TGA analyses of these complexes at a heating rate of 5 °C/min and nanoparticle syntheses using them as precursors. The TGA plot of the Fe(II) oleate showed a weight loss onset at around 185 °C, but continued up to 270 °C, suggesting a very slow decomposition process. Compared to the TGA plot of the Fe(III) oleate complex, the secondary weight loss around 230 °C was not apparent (Figure S5a, Supporting Information). This is consistent with our electronic structure calculations of the Fe(II) oleate complex, where the Fe(II) oleate complex has two stable structures with symmetric ligand arrangements (Figure 5a). The symmetrical arrangements indicate similar binding energies or dissociation temperatures of these two ligands. A very small weight loss region right below 300 °C exhibits a slightly different weight loss rate, likely from the oxidation of Fe(II) oleate during synthesis or experimental operation. This oxidation process can also be visualized by the color change of the complex from dark to brown. The TGA plot of the Fe(II)/Fe(III) oleate complex mixture did not show much difference from the decomposition behavior of the Fe(III) complex (Supporting Information Figure S5a) with two weight loss onsets below 300 °C. Alternatively, we also performed TGA analyses on commercially available, stable Fe(II) and Fe(III) stearate complexes (Figure S5b, Supporting Information), where the difference in weight losses can be clearly seen with one weight loss onset for the Fe(II) complex and two for the Fe(III) complex below 300 °C.

Comparable experiments were also performed using Fe(II) oleate and a Fe(II)/Fe(III) oleate mixture as precursors under similar conditions. Irregular shaped and somehow aggregated nanoparticles were observed when Fe(II) oleate was used as a precursor (Figure 5b). In contrast, a mixture of small irregular nanoparticles and nanowhiskers was formed when using this complex mixture as the precursor under identical reaction conditions (Figure 5c). This observation indirectly confirms the importance of the third ligand in directing the growth of iron oxide nanowhiskers.

It is well-known that selective adsorption of ligands on the nanoparticle crystalline planes can significantly alter the growth pathways of nanoparticles, subsequently leading to the control of nanoparticle geometries.[47] Experiments using surfactant mixtures were performed to understand the effects of alternate ligands on the nanowhisker formation. The surfactant mixtures were oleic acid-OA/trioctylphosphine oxide-TOPO and OA/oleyamine-ON, where TOPO has a weaker binding to iron oxide nanoparticle surfaces than OA, while ON has a stronger binding.[48] Both experiments produced nanoparticles with whisker morphologies (Supporting Information Figure S6). The FTIR spectra of these nanowhiskers exhibited primarily the characteristic bands of carboxylates with no detectable signals of TOPO or ON. The frequency difference between the asymmetrical (ν_{as}) and symmetrical (ν_s) COO^- vibrations for both samples also fell within the range of the bridging coordination mode. This study provides additional evidence that the remaining ligand of the iron oleate complex plays a critical role during the nanostructure formation and that the growth process was not altered by the other ligands.

On the basis of all these observations, we propose that the nanowhisker formation was directed by the third ligand. The interaction between the third ligand plays an important role in directing the formation of the 1D nanostructure, where the Fe−O part of the complex forms the inorganic backbone and surrounded by the oleate ligands (Figure S7a, Supporting Information). Additionally, to verify our hypothesis we performed similar reactions at 230 °C using commercially available, stable precursors (e.g., Fe(II) and Fe(III) stearate complexes). Interestingly, very similar results were obtained with the formation of spheres for Fe(II) stearate and 1D nanostructures

dx.doi.org/10.1021/nl200136j |*Nano Lett.* 2011, 11, 1141–1146

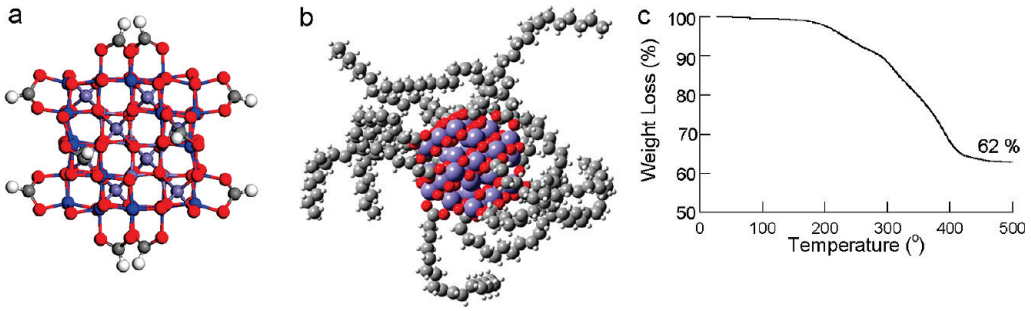

Figure 6. (a) Relaxed structure of $Fe_{39}O_{62}(HCOO)_{12}$, (b) structure of a simulated iron oxide nanocluster structure with oleate ligand shell, and (c) a TGA plot of iron oxide nanowhiskers.

for Fe(III) stearate (Supporting Information Figure S7b,c). However, the presence of cavities within the 1D nanostructures needs further investigation.

A similar ligand-directed growth mechanism from single-ligand complexes has been reported for the formation of ultrathin gold nanowires.[7−9] The fundamental building block of the nanowhiskers is hypothesized to be stable iron oxide nanoclusters with a ligand shell based on the diameter of the nanowhiskers. Iron oxide nanoclusters have been previously observed in many studies and exhibit magnetic transition characteristics of molecular magnets to bulk magnetism.[49−51] It has been previously reported that iron carboxylate complexes could self-assemble into crystalline films by direct evaporation and without heat treatment.[52]

Accordingly, we performed electronic structure calculations on a hypothesized iron oxide nanocluster-oleate structure, $Fe_{39}O_{62}(HCOO)_{12}$ to understand its structural geometry and stability (Figure 6a). This structure has a 1.1 nm iron oxide nanocluster center with S_6 symmetry and a ligand shell. The ligands were simplified as HCOOH to reduce the workload from the long hydrocarbon chains (with an assumption that the chain length would only mildly affect the nanocluster geometry, at most). In the iron oxide nanocluster center, the 39 Fe^{3+} cations occupy 8 tetrahedral sites and 7 octahedral sites in the inner core, and 12 pentahedral sites (blue) and 12 octahedral sites (blue) on the surface, forming 24 Fe−O coordinate bonds in a bridging mode with 12 $HCOO^-$ ligands. The bridging mode coordination bonds are consistent with the FTIR analysis of the oleate coated nanowhiskers, yielding a $RCOO^-$ to Fe_2O_3 ratio of 1:1.6. The bridging bonds of the relaxed structure (Figure 6a) can be clearly identified. After relaxation, the oleate ligands were introduced to the nanocluster core, in order to present the configuration of the ligand shell complex (Figure 6b). It must be recognized that with a complex structure like Figure 6b, the optimization likely only leads to a local minimum when considering the complete three-dimensional phase space. Thus, we refer to our model as a "relaxed" representation of the cluster.

The ratio of the capping ligands to Fe_2O_3 can be experimentally determined using a TGA measurement. The weight loss started around 200 °C and gradually continued to 400 °C. The early weight loss can be ascribed to the decomposition of oleate, as suggested by the TGA plot of the oleate complex at a slower heating rate (1 °C/min) (Figure S1a, Supporting Information). The weight loss above 300 °C is from desorption or vaporization of oleate ligands. This thermal behavior is similar to that of oleic acid coated iron oxide nanoparticles.[53] The final residue mass of the TGA measurements was about 62% after heating-up to over 500 °C (Figure 6c). The mass percentage divided by the molecular weight of Fe_2O_3 and the oleate ligand led to a molecular ratio of $RCOO^-$ to Fe_2O_3 of about 1:2.8. The ratio (1:1.6) of RCOO to Fe_2O_3 for the simulated nanocluster (1.1 nm) was larger than that of the experimental estimation (1:2.8) because the size of the simulated nanocluster was smaller than the diameter of the nanowhiskers. With increasing cluster size, the ratio of RCOO to Fe_2O_3 will decrease because of the decreasing surface atom percentage, which requires less ligands to saturate the surface Fe sites. Our somewhat reduced simulation model was chosen for computational efficiency.

In summary, thin iron oxide nanowhiskers have been successfully synthesized through selective decomposition of the iron oleate complex. The major discovery of this work is that the ligand coordination microenvironments have been found to play an important role in the nanowhisker formation, which has not been studied previously. The different ligand environments were probed by electronic structure calculations and TGA measurement. Subsequently, a ligand-directed growth mechanism for the iron oxide nanowhisker formation was proposed and stable iron oxide nanoclusters were hypothesized to be the basic building blocks. Accordingly, we performed electronic structure calculations on a hypothesized nanocluster, which agrees well with our experimental observation. We expect that similar nanostructures can be synthesized for other metals once proper ligands and decomposition temperatures are identified. The studies of Fe(II) and Fe(III) stearate provide a great support of our hypothesis. The formation of the nanowhiskers provides a unique shape-control example of nanostructures based on a deep understanding of the precursor ligand chemistry, offering additional insights into nanoparticle synthesis. In particular, the effects of the ligand microenvironment present another synthetic strategy for nanoparticle shape control.

■ ASSOCIATED CONTENT

Supporting Information. Experimental details; TGA plots of isothermal and slower heating rate processes; X-ray diffraction pattern of iron oxide nanowhiskers; time and temperature-dependent study, TGA plots of Fe(II) oleate, Fe(II)/Fe(III) oleate mixture, Fe(II) stearate, and Fe(III) stearate; alternative ligand effects on the nanowhisker formation; and schematic drawing of growth mechanism and experimental results using Fe(II) and Fe(III) stearate as precursors. This material is available free of charge via the Internet at http://pubs.acs.org.

■ AUTHOR INFORMATION

Corresponding Author

*(Y.B.) E-mail: ybao@eng.ua.edu. Phone: (205) 348-9869. Fax: (205) 348-7558. (C.H.T.) E-mail: hturner@eng.ua.edu. Phone: (205) 348-1733. Fax: (205) 348-7558.

■ ACKNOWLEDGMENT

This work was supported in part by NSF-DMR 0907204 and an ORAU Junior Faculty Enhancement Award. We acknowledge the UA Central Analytical Facility (CAF) and the Biological Science Department for the use of TEM. We thank the UA-MINT center for the use of the AGM. We thank NSF award (0925445) for the use of Raman Instrument. C.H.T. acknowledges support from an NSF CAREER Award (0747690). Supercomputer resources were provided by the Alabama Supercomputer Center and the NCSA TeraGrid. A portion of this research was performed using EMSL, a national scientific user facility sponsored by the Department of Energy's Office of Biological and Environmental Research and located at Pacific Northwest National Laboratory. The authors also thank Dr. Steve Ritchie and Professor Jin Zhang for useful discussions.

■ REFERENCES

(1) Cohen-Karni, T.; Qing, Q.; Li, Q.; Fang, Y.; Lieber, C. M. *Nano Lett.* **2010**, *10*, 1098–1102.
(2) Chen, J.; Wiley, B. J.; Xia, Y. *Langmuir* **2007**, *23*, 4120–4129.
(3) Baker, J. L.; Widmer-Cooper, A.; Toney, M. F.; Geissler, P. L.; Alivisatos, A. P. *Nano Lett.* **2010**, *10*, 195–201.
(4) Xia, Y.; Xiong, Y.; Lim, B.; Skrabalak, S. E. *Angew. Chem., Int. Ed.* **2009**, *48*, 60–103.
(5) Lee, E. P.; Peng, Z.; Cate, D. M.; Yang, H.; Campbell, C. T.; Xia, Y. *J. Am. Chem. Soc.* **2007**, *129*, 10634–10635.
(6) Cademartiri, L.; Ozin, G. A. *Adv. Mater.* **2009**, *21*, 1013–1020.
(7) Li, Z.; Tao, J.; Lu, X.; Zhu, Y.; Xia, Y. *Nano Lett.* **2008**, *8*, 3052–3055.
(8) Wang, C.; Sun, S. *Chem.--Asian J.* **2009**, *4*, 1028–1034.
(9) Poudyal, N.; Chaubey, G. S.; Nandwana, V.; Rong, C.; Yano, K.; Liu, J. *Nanotechnology* **2008**, *19*, No. 355601-1−4.
(10) Huo, Z.; Tsung, C.; Huang, W.; Zhang, X.; Yang, P. *Nano Lett.* **2008**, *8*, 2041–2044.
(11) Chen, M.; Pica, T.; Jiang, Y.; Li, P.; Yano, K.; Liu, J.; Datye, A. K.; Fan, H. *J. Am. Chem. Soc.* **2007**, *129*, 6348–6349.
(12) Huo, Z.; Tsung, C.; Huang, W.; Fardy, M.; Yan, R.; Zhang, X.; Li, Y.; Yang, P. *Nano Lett.* **2009**, *9*, 1260–1264.
(13) Yu, T.; Joo, J.; Park, Y. I.; Hyeon, T. *J. Am. Chem. Soc.* **2006**, *128*, 1786–1787.
(14) Lee, C. M.; Jeong, H. J.; Lim, S. T.; Sohn, M. H.; Kim, D. W. *ACS Appl. Mater. Interfaces* **2010**, *2*, 756–759.
(15) Wang, Y.; Yang, H. *Chem. Eng. J.* **2009**, *147*, 71–78.
(16) Pankhurst, Q. A.; Connolly, J.; Jones, S. K.; Dobson, J. *J. Phys. D: Appl. Phys.* **2003**, *36*, R167–R181.
(17) Veiseh, O.; Gunn, J. W.; Zhang, M. *Adv. Drug Delivery Rev.* **2010**, *62*, 284–304.
(18) Park, J. H.; von Maltzahn, G.; Zhang, L.; Schwartz, M. P.; Ruoslahti, E.; Bhatia, S. N.; Sailor, M. J. *Adv. Mater.* **2008**, *20*, 1630–1635.
(19) Park, J.; An, K. J.; Hwang, Y. S.; Park, J. G.; Noh, H. J.; Kim, J. Y.; Park, J. H.; Hwang, N. M.; Hyeon, T. *Nat. Mater.* **2004**, *3*, 891–895.
(20) Shavel, A.; Rodriguez-Gonzalez, B.; Spasova, M.; Farle, M.; Liz-Marzan, L. M. *Adv. Funct. Mater.* **2007**, *17*, 3870–3876.
(21) Shavel, A.; Rodriguez-Gonzalez, B.; Pacifico, J.; Spasova, M.; Farle, M.; Liz-Marzan, L. M. *Chem. Mater.* **2009**, *21*, 1326–1332.
(22) Shavel, A.; Liz-Marzan, L. M. *Phys. Chem. Chem. Phys.* **2009**, *11*, 3762–3766.
(23) Hai, H.; Yang, H.; Kura, H.; Hasegawa, D.; Ogata, Y.; Takahashi, M.; Ogawa, T. *J. Colloid Interface Sci.* **2010**, *346* (1), 37–42.
(24) Kovalenko, M. V.; Bodnarchuk, M. I.; Lechner, R. T.; Hesser, G.; Schaffler, F.; Heiss, W. *J. Am. Chem. Soc.* **2007**, *129*, 6352–6353.
(25) Xu, Z.; Shen, C.; Tian, Y.; Shi, X.; Gao, H. *Nanoscale* **2010**, *2*, 1027–1032.
(26) Kim, D.; Park, J.; An, K.; Yang, N.; Park, J. G.; Hyeon, T. *J. Am. Chem. Soc.* **2007**, *129*, 5812–5813.
(27) Kwon, S. G.; Piao, Y.; Park, J.; Angappane, S.; Jo, Y.; Hwang, N. M.; Park, J. G.; Hyeon, T. *J. Am. Chem. Soc.* **2007**, *129*, 12571–12584.
(28) Lopez-Cruz, A.; Lopez, G. E. *Mol. Phys.* **2009**, *107*, 1799–1804.
(29) Garg, A. N.; Lanjewar, R. B. *J. Radioanal. Nucl. Chem.* **1995**, *199*, 443–452.
(30) Davis, R.; Schltz, H. P. *J. Org. Chem.* **1962**, *27*, 854–857.
(31) Ganguly, A.; Kundu, R.; Ramanujachary, K. V.; Lofland, S. E.; Das, D.; Vasanthacharya, N. Y.; Ahmad, T.; Ganguli, A. K. *J. Chem. Sci.* **2008**, *120*, 521–528.
(32) Roca, A. G.; Morales, M. P.; Serna, C. J. *IEEE Trans. Magn.* **2006**, *42*, 3025–3029.
(33) Kwon, K. W.; Lee, B. H.; Shim, M. *Chem. Mater.* **2006**, *18*, 6357–6363.
(34) Park, J. N.; Zhang, P.; Hu, Y.; McFarland, E. W. *Nanotechnology* **2010**, *21*, 225708–1−8.
(35) Jia, C.; Sun, L.; Luo, F.; Han, X.; Heyderman, L. J.; Yan, Z.; Yan, C.; Zheng, K.; Zhang, Z.; Takano, M.; Hayashi, N.; Eltschka, M.; Klaui, M.; Rudiger, U.; Kasama, T.; Cervera-Gontard, L.; Dunin-Borkowski, R. E.; Tzvetkov, G.; Raabe, J. *J. Am. Chem. Soc.* **2008**, *130*, 16968–16977.
(36) Teng, X.; Yang, H. *J. Mater. Chem.* **2004**, *14*, 774–779.
(37) Guardia, P.; Batlle-Brugal, B.; Roca, A. G.; Iglesias, O.; Morales, M. P.; Serna, C. J.; Labarta, A.; Batlle, X. *J. Magn. Magn. Mater.* **2007**, *316*, E756–E759.
(38) Kachkachi, H.; Ezzir, A.; Nogues, M.; Tronc, E. *Eur. Phys. J. B* **2000**, *14*, 681–689.
(39) Koseoglu, Y.; Kavas, H.; Aktas, B. *Phys. Status Solidi A* **2006**, *203*, 1595–1601.
(40) Millan, A.; Urtizberea, A.; Silva, N. J. O.; Palacio, F.; Amaral, V. S.; Snoeck, E.; Serin, V. *J. Magn. Magn. Mater.* **2007**, *312*, L5–L9.
(41) Koseoglu, Y.; Kavas, H. *J. Nanosci. Nanotechnol.* **2008**, *8* (2), 584–590.
(42) Iglesias, O.; Labarta, A. *Phys. Rev. B* **2001**, *63*, 184416–11.
(43) Nakamoto, K. *Infrared and Raman Spectra of Inorganic and Coordination Compounds*, 4th ed.; John Wiley & Sons: New York, 1986.
(44) Abrahamson, H. B.; Lukaski, H. C. *J. Inorg. Biochem.* **1994**, *54*, 115–130.
(45) Lu, Y.; Miller, J. D. *J. Colloid Interface Sci.* **2002**, *256*, 41–52.
(46) Culita, D. C.; Patron, L.; Teodorescu, V. S.; Balint, L. *J. Alloys Compd.* **2007**, *432*, 211–216.
(47) Hyeon, T. *Chem. Commun.* **2003**, 927–934.
(48) Palchoudhury, S.; Xu, Y.; An, W.; Turner, C. H.; Bao, Y. *J. Appl. Phys.* **2010**, *107*, 09B311–09B313.
(49) Gatteschi, D.; Caneschi, A.; Pardi, L.; Sessoli, R. *Science* **1994**, *265*, 1054–1058.
(50) Canada-Vilalta, C.; O'Brien, T. A.; Pink, M.; Davidson, E. R.; Christou, G. *Inorg. Chem.* **2003**, *42*, 7819–7829.
(51) Christmas, C. A.; Tsai, H. L.; Pardi, L.; Kesselman, J. M.; Gantzel, P. K.; Chadha, R. K.; Gatteschi, D.; Harvey, D. F.; Hendrickson, D. N. *J. Am. Chem. Soc.* **1993**, *115*, 12483–12490.
(52) Popescu, M.; Turta, C.; Meriacre, V.; Zubareva, V.; Gutberlet, T.; Bradaczek, H. *Thin Solid Films* **1996**, *274*, 143–146.
(53) Huang, J.; Parab, H. J.; Liu, R.; Lai, T.; Hsiao, M.; Chen, C.; Sheu, H.; Chen, J.; Tsai, D.; Hwu, Y. K. *J. Phys. Chem. C* **2008**, *112*, 15684–15690.